EIGHTH EUROPEAN ROTORCRAFT FORUM

Paper No. 9.2

FLUCTUATING FORCES AND ROTOR NOISE DUE TO MAIN ROTOR - TAIL ROTOR INTERACTION

J. SCHREIER

INSTITUT FÜR LUFT- UND RAUMFAHRT DER
RHEINISCH-WESTFÄLISCHEN TECHNISCHEN HOCHSCHULE AACHEN
GERMANY

August 31 through September 3, 1982

AIX-EN-PROVENCE, FRANCE

ASSOCIATION AERONAUTIQUE ET ASTRONAUTIQUE DE FRANCE

FLUCTUATING FORCES AND ROTOR NOISE

DUE TO MAIN ROTOR - TAIL ROTOR INTERACTION

J. SCHREIER
Institut für Luft- und Raumfahrt der
Rheinisch-Westfälischen Technischen Hochschule Aachen
D-5100 Aachen, Germany

Abstract

The paper is concerned with the helicopter noise which is generated by the interaction of the tip vortices of the main rotor with the tail rotor. This interaction was simulated by a test facility with two rotors. Sound pressure levels and noise spectra have been measured under various conditions. The unsteady forces on the tail rotor blades as well as the radiated sound field were calculated. Measured and calculated data show a reasonable agreement.

1. Introduction

Efforts to reduce the noise emission of aircraft are of great importance. Much progress has been made in this respect during the last 15 years, as far as fixed wing aircraft are concerned. Helicopters however have different noise problems; those machines which are operated today have an intensive noise radiation.

Helicopter noise causes a strong subjective loudness which results from discrete tones in its spectrum. The frequencies of these tones are determined by the blade passage frequencies of the main and tail rotor and the harmonics. During certain flight conditions another additional noise mechanism which generates the so called "impulsive noise" is especially intensive. One source of this "impulsive noise" is the tail rotor. Here the vortices, which are shed by the tips of the main rotor are cut by the blades of the tail rotor (figure 1). These vortices induce velocities that cause fluctuations of the angle of attack and of the dynamic pressure at the tail rotor blades. These changes in the inflow conditions, in turn, cause unsteady forces on the blades which increase the noise radiation.

The noise radiation, caused by the interaction of tip vortex and tail rotor was studied in the ILR. Unfortunately it was not possible to take measurements on an original helicopter. For this reason a test bench was built, which simulated the interaction of the main rotor tip vortex and the tail rotor. Sound pressure measurements were made in a reverberation room.

A computer model was developed which determines the velocity-pertubations which occur during this interaction at the tail rotor blades. From these velocitiy pertubations the unsteady blade forces were calculated. Using the force oscillations as a starting point a method for calculating the radiated sound field was developed.

2. Apparatus And Procedure

2.1 Rotor Test Facilities

A sketch of the mentioned test facility can be seen in figure 2. It consists of two separate rotor test facilities. One component of this apparatus is made up of an original tail rotor of a helicopter UH-1D by Bell (diameter 2.6 m). This rotor was driven by a 65 kW dc motor.

The second rotor was used to generate the tip vortices. This vortex generator had a diameter of 1.6 m. Its speed was continuously variable. The interaction of the tip vortex and the tail rotor, which is determined by the set-up of the test facilities, simulates the interaction as it occurs on the original helicopter. Figure 2 shows the tip vortex generated by a blade. Also the areas can be seen where the tail rotor cuts this vortex.

2.2 Acoustic Technique of Measurement

The acoustic measurements took place in a reverberation chamber. If a reverberation chamber is excited with a white noise, a sound field will be formed, which has constant energy density at every point. However, in this experiment the room was excited by discrete tones. Only a few standing waves are formed, thus one can no longer assume a sound field with a constant energy density. For this reason it was necessary to average the sound pressures measured at many locations. The problem was resolved by moving the microphone over a circle with the radius r_m = 3 m and then integrating the sound pressure over one revolution (80 sec.).

3. Results of the Acoustic Measurements

The influence of the following parameters on the noise generation of the tail rotor was studied:

1. Tail rotor rpm (n_T)
2. Blade angle (ϑ_T)
3. Vortex generator rpm (n_V)
4. Strength of the tip vortex (Γ_V)

Figure 3 shows the overall sound pressure level OASPL as a function of tail rotor rpm. Region (1) and Region (2) are valid for the undisturbed and the disturbed case respectively. For the undisturbed rotor the OASPL is strongly dependent on ϑ_T. However, in the case of a disturbed rotor, this dependence cannot be found. The overall sound pressure level increases as about the third power of the blade-tip velocity.

In order to be able to determine the frequency region in which this noise appears, the spectra are plotted in figure 4 for the undisturbed case (graph 1) and the disturbed case (graph 2). It can be seen that, because of this blade-vortex interaction, the sound level is increased in the region from low frequencies up to 3000 Hz. For the higher frequencies no difference worth mentioning can be found. Since those components which determine the overall sound pressure level are below 1000 Hz, only this region will be studied in the following frequency analysis.

Figure 5 shows the spectra for the undisturbed (graph 1) and for the disturbed rotor (graph 2). Here the tail rotor and the vortex generator had the same number of revolutions per minute. It can be seen, that the sound level of the disturbed case is up to 20 dB higher than the value for the undisturbed case. Only the fundamental frequency and its first harmonic remain unchanged. The increase in the sound level is not only limited to the blade passage noise, but the level of the broad band noise is also increased considerably. This means that the blade-vortex interaction does not only cause those force variations at the rotor blades which are periodic with the rotor rpm's, but that there also are arbitrary force variations. These are caused by an increase in the turbulence in the rotor inflow which results in an increase in the broad band noise.

Figure 6 shows the spectra of the tail rotor noise for rpm different for the rotors. It can be seen that now additional tones grow up besides the blade passage harmonics. Above 300 Hz these tones have about the same noise level as the blade passage harmonics.

The influence of the strength of the tip vortex is demonstrated in figure 7. Here, sound pressures are shown as a function of the tail rotor rpm. In this case the vortex generator was operated at a constant speed (n_V = 750 rpm) with different blade angles ($\vartheta_V = 38^\circ$ or $\vartheta_V = 25^\circ$). Also, for comparison, the graph for the undisturbed tail rotor has been included. The figure shows that a stronger vortex also increases the noise radiation.

4. Calculations of the Velocity Disturbances

For the calculation of the velocity disturbances, which are induced by a vortex in the tail rotor plane, the model of a viscous vortex is used. For the tangential velocity component v_t of the vortex, the following expression applies:

$$(1) \qquad v_t = \frac{\Gamma}{2\pi r} \left\{1 - e^{-r^2/(\nu_t t)}\right\}$$

where Γ = vortex strength (m^2/s)

t = age of the vortex (s)

ν_t = vortex viscosity (m^2/s)

A relation derived by OWEN /lit. 1/ was used for calculating the vortex viscosity for an aged vortex:

$$(2) \qquad \nu_t = 0.588 \sqrt{\Gamma \nu}$$

where ν = kinematic viscosity (m^2/s)

A vortex, traversing the plane of the tail rotor, induces a velocity at every point P in the plane, which depends, in magnitude as well as in direction, on the distance between the point P and the vortex center. When calculating the flow

velocities, only those components are taken into account which are vertically aligned with respect to the leading edge of the blade, since changes in the angle of attack and in the dynamic pressure are mainly influenced by these components.

In order to be able to calculate the vortex induced velocity at every point P in the plane of the tail rotor, the position of the vortex has to be determined first. Figure 8 shows a vortex with an arbitrary relative position with respect to the plane of the tail rotor. The position of the center of the vortex in the plane is fixed by the radius r_Γ and the angle X.

The direction of the vortex axis can be determined by the angle of inclination ξ_C and the azimuth angle η_C, which is the angle between the x-axis and the projection of the vortex axis on the plane of the rotor. Also included in figure 8 is the vortex induced velocity $\vec{v}_t$ at a blade element. The following two components of $\vec{v}_t$ which are vertical to the leading edge of the blade are needed for the subsequent calculation of the blade forces:

v in the rotor plane
w vertical to the rotor plane

The calculation of the components v and w is done with the help of vector-algebra in a coordinate system which is fixed at the leading edge of the blade element. Its three axis are:

x_B parallel to the leading edge
y_B in the rotor plane vertical to the leading edge
z_B vertically to the rotor plane

The position of a point on the vortex axis is given by the following vector equation:

$$(3) \qquad \vec{w} = \vec{r}_{\Gamma B} + \lambda \vec{w}_l$$

where $\vec{r}_{\Gamma B}$ vector from the origin of the coordinate system to the point, at which the vortex axis traverses the plane of the rotor
$\vec{w}_l$ unit directional vector of the vortex axis
λ parameter

For the vectors $\vec{r}_{\Gamma B}$ and $\vec{w}_l$ the following relation is valid:

$$(4) \qquad \vec{r}_{\Gamma B} = \begin{pmatrix} r_\Gamma \cos(X - \gamma) - r \\ r_\Gamma \sin(X - \gamma) \\ 0 \end{pmatrix} \quad ; \quad \vec{w}_l = \begin{pmatrix} \sin\xi \cos\eta \\ \sin\xi \sin\eta \\ \cos\xi \end{pmatrix}$$

The velocity vector $\vec{v}_t$ can be calculated

$$(5) \qquad \frac{\vec{v}_t}{|v_t|} = - \frac{\vec{r}_w \cdot \vec{w}_1}{|r_w|}$$

after determing $\vec{r}_w$ the position vector which intersects the vortex axis at a right angle (r_w = distance of blade element from the vortex axis)

$$(6) \qquad \vec{r}_w = \vec{r}_{\Gamma B} - (\vec{r}_{\Gamma B} \vec{w}_1) \vec{w}_1$$

Applying eqs 1 - 6 yields the components of the induced velocities

$$(7) \qquad \vec{v}_t = \begin{pmatrix} u \\ v \\ w \end{pmatrix} = - \frac{1}{r_w} \left\{ \frac{\Gamma}{2\pi r_w} \left(1 - e^{-r_w^2/\nu_t t}\right) \right\} \begin{pmatrix} r_\Gamma \sin(X - \gamma) \cos\xi \\ (r_\Gamma \cos(X - \gamma) - r) \cos\xi \\ \{(r_\Gamma \cos(X - \gamma) - r) \sin\eta - \\ \quad - r_\Gamma \sin(X - \gamma) \cos\eta\} \sin\xi \end{pmatrix}$$

Tail Rotor in the Downwash of the Vortex Generator

Additionally, the tail rotor is also disturbed by the downwash field of the vortex generator. To include the influence of the downwash field in the acoustic calculations, the following simplifications have been made:

1. The downwash field is of a constant magnitude in the inner region and decreases with a cosine-function at the outer edge
2. The downwash field is not influenced by the tail rotor.

The vortex generator is set up in such a way, that there is no downwash component vertical to the plane of the tail rotor. Again, the calculation of the forces use only the velocity component vertical to the leading edge of the blade.

5. Calculation of the Unsteady Blade Forces

To calculate the unsteady forces, the velocity pertubations - due to the tip vortex and the downwash - are superposed. Resulting velocity components are shown in figure 9 for three blade elements. The path of the vortices, as they are included in the drawing, was determined with the help of smoke pictures.

The velocity components are Fourier analysed. This analysis yields the velocity spectrum and the corresponding phase angle. Starting out with the velocity amplitudes, the unsteady blade forces were calculated using a method by NAUMANN and YEH /lit. 2/. This method applies a theory in which only two-dimensional effects are taken into account. Furthermore, nonviscous and incompressible flow is presumed.

Figure 10 shows the unsteady blade forces for the three blade elements.

6. Calculation of the Radiated Sound Field

The calculation of the sound field is based on the inhomogeneous wave equation, as formulated by LIGHTHILL /lit. 3/. In this equation three different acoustic source terms are represented. Concerning the rotor noise generation at lower subsonic rotor tip speeds - as regarded in this paper -, two of these source terms are inefficient: that is the effect of mass displacement of the rotating blades and the effect of turbulent momentum exchange in the boundary layers and the wakes of the blades. As the dominant source term the effect of the fluctuating forces F_i^* remains. Now the wave equation can be written as

$$(8) \qquad \frac{1}{a^2}\frac{\partial^2 p}{\partial t^2} - \frac{\partial^2 p}{\partial x_i^2} = -\frac{\partial F_i^*}{\partial x_i}$$

with the sound pressure p, the speed of sound a, the time t and x_i a three-dimensional cartesian coordinate (see figure 11).

Lighthill gave the solution of this wave equation in the form

$$(9) \qquad p = \frac{1}{4\pi}\frac{\partial}{\partial x_i}\int \left(\frac{F_i}{R}\right) dA$$

where p is the sound pressure at the position of the observer P. R is the distance from source Q to observer P and dA is an element of the rotor area. F_i are now the components of the force per unit area acting on fixed points in the rotor area. F is generated as the reaction of lift and drag of the rotor blades. The square brackets around F_i/R imply the evaluation at the retarded time $\tau = t - R/a$. To integrate over the rotor area requires an integration over the radius R_T and over the angle γ around the rotor.

LIGHTHILL showed in /lit. 3/ that the differentiation with respect to x_i in (9) and the dropping of a term which goes with the inverse square of the distance (R) from the source to the point P yields for large R the equation

$$(10) \qquad p = \frac{1}{4\pi a}\int_0^{2\pi}\int_0^{R_T} \frac{\vec{R}}{R^2}\frac{\partial}{\partial t}\left(\vec{F}\left(\vec{r}, t - \frac{R}{a}\right)\right) r\, dr\, d\gamma$$

At first, the fluctuations shall be analysed for a rotor with undisturbed inflow. In this case the blade forces do not change during the revolution. However, there are fluctuations in F_i at a fixed point in space, every time a blade passes by. These fluctuations are periodical with the blade passage frequency B·N, where B is the blade number and N is the number of revolutions per second.

These fluctuations can be Fourier analysed having discrete frequencies

$$(11) \qquad f_m = m\, B\, N$$

with the harmonic order m. The Fourier coefficients depend on the shape of the F_i-pulses. This shape is determined by the pressure distribution acting on the blade element.

However if the inflow is disturbed, the aerodynamic force L on a blade element which traverses this disturbance is not constant. Now the assumption is made that the inflow is locally disturbed but is not a function of time. Then the fluctuation of L is periodic with the frequency N. Because of the periodicity L can be Fourier analysed.

$$(12) \quad L(r,\gamma) = L_{St}(r) + \sum_{n=1}^{\infty} L_n(r) \cos\left(n\gamma - \eta_n(r)\right)$$

At a fixed point Q in the rotor plane the blade force L leads to the force F:

$$(13) \quad F(r, \gamma, t) = \frac{L_{St}(r)\, B}{2\pi r} \left\{1 + \sum_{m=1}^{\infty} |\psi_m| \left\{ \sum_{n=0}^{\infty} \frac{L_n(r)}{L_{St}(r)} \cdot \right.\right.$$

$$\cdot \left(\cos\left(mB\Omega t - q_+\gamma + \varphi_n - \Delta_m\right) + \right.$$

$$\left.\left. + \cos\left(mB\Omega t - q_-\gamma - \varphi_n - \Delta_m\right)\right)\right\}\right\}$$

$L_{St}(r)$ = steady blade force (per unit width of the blade element)

$L_n(r)$ = unsteady blade force (per unit width of the blade element)

B = number of blades of the rotor

$q_{\pm}$ = $(mB \pm n)$

$|\psi|_m$ = magnitude of the spectral function, which results from the shape of the chordwise pressure distribution

φ_n, Δ_m = phase angle

Ω = angular velocity of the rotor

To calculate the radiated noise of the rotor the contributions of the force-fluctuations at all fixed points in the rotor area have to be integrated while considering the phase relations. For this purpose the method of LOWSON /lit. 4/ and WRIGHT /lit. 5/ had to be extended. The following equation for the pressure of the m-th sound harmonic is deduced in /lit. 6/.

$$(14)\quad p_m(t) = \frac{mB\Omega B}{4\pi aA}\int_0^{R_T} |\psi_m(r)| \sum_{n=0}^{\infty} L_n(r)\,\{J_{q_-}(z)\sin\left[mB\Omega\left(t-\frac{A}{a}\right)-q_-\left(\Phi-\frac{\pi}{2}\right)-\eta_n-\Delta_m\right]\cdot\left(\cos\Theta\cos\beta - q_-\frac{a}{mB\Omega r}\sin\beta\right)+$$

$$+ J_{q_+}(z)\sin\left[mB\Omega\left(t-\frac{A}{a_o}\right)-q_+\left(\Theta-\frac{\pi}{2}\right)+\varphi_n-\Delta_m\right]\cdot$$

$$\cdot\left(\cos\Theta\cos\beta - \frac{q_+ a}{mB\Omega_r}\sin\beta\right)\}\,dr$$

A = distance from point P to the origin of the coordinate system

Φ, Θ = angle of the point P

tg β = drag/thrust

$J_{q\pm}$ = Bessel function of order q_+ or q_-

$z = \frac{mB\, r \sin\Theta}{a}$ = argument of the Bessel function

Equation 14 was solved numerically.

The sound pressure level of the tail rotor noise was measured in a reverberation room. Because of the reflections which occur in a reverberation room, the directional characteristic of a radiated sound field gets lost. For this reason, only sound power levels can be compared with calculated data. The sound power was calculated using

$$(15)\quad P = \frac{1}{T}\int_0^T dt \int_{\text{surface of sphere}} \frac{p_m(t)^2}{\rho a}\,dS$$

7. Comparison of Measurements and Calculations

From figure 12 can be seen that, with the exception of the blade passage frequency, there is a good agreement between measurements and calculations.

The application of this model for the computation of the sound field of a real helicopter needs the knowledge of the vortex parameters (Γ_o, v_t) and the path of the vortices through the tail rotor plane. These informations can be achieved by measurements or theoretical assumptions.

8. Summary

The paper is concerned with noise generated by helicopter tail rotors. In particular, the influence of the tip vortices of the main rotor has been investigated by experiments and calculations.

Since an original helicopter was not available for experiments, a test facility was built, where the tip vortex of the main rotor was simulated with the help of a smaller rotor. The tail rotor was an original component of a helicopter UH-1D.

Furthermore, a method has been developed for the calculation of the velocity pertubations which are caused by the tip vortex and the downwash of the vortex generating rotor. Using these pertubations the unsteady blade forces were determined with a singularity method. These forces served as input for a computer program with which the sound field, generated by the tail rotor, was calculated.

The following conclusions can be drawn from experiments and calculations:

(1) Unsteady forces on the tail rotor blades induced by passing vortices, cause a considerable increase of sound radiation over the spectrum of blade passage harmonics.

(2) If the speed of the tail rotor is increased, the sound pressure is nearly proportional to the third power of the blade tip velocity. The pitch angle of the tail rotor blades has no influence on the interaction noise.

(3) A doubling of the tip vortex strength gives an increase of the noise power level of 3 dB.

(4) The calculations of the noise spectrum show a fairly good agreement with the experimental results.

9. References

1. P.R. Owen, The Decay of a Turbulent Trailing Vortex, Aeronautical Quarterly Vol. XXI, p 69 (1970)

2. H. Naumann and H. Yeh, Lift on Pressure Fluctuations of a Cambered Airfoil under Periodic Gusts and Applications in Turbomachinery, Paper 72-6T-30, ASME (1972)

3. M.J. Lighthill, On Sound Generated Aerodynamically, Proc. Roy. Soc. A 211, p 564 (1952)

4. M.V. Lowson, Theoretical Studies of Compressor Noise, NASA CR-1287 (1969)

5. S.E. Wright, Sound Radiation from a Lifting Rotor Generated by Asymetric Disk Loading, J. of Sound and Vibr., Vol. 9 (1969)

6. R. Staufenbiel, J. Schreier, G. Neuwerth, Lärmerzeugung von Hubschraubern unter besonderer Berücksichtigung des Heckrotors, Forschungsbericht des Landes NRW, Nr. 3144, Fachgruppe Umwelt/Verkehr (1982)

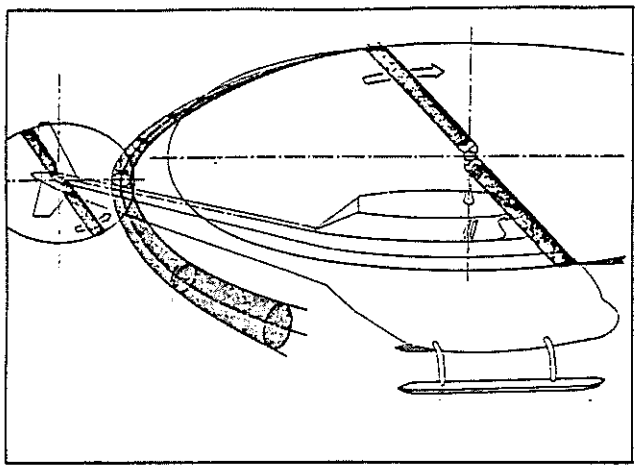

Fig. 1 Interaction between main rotor and tail rotor

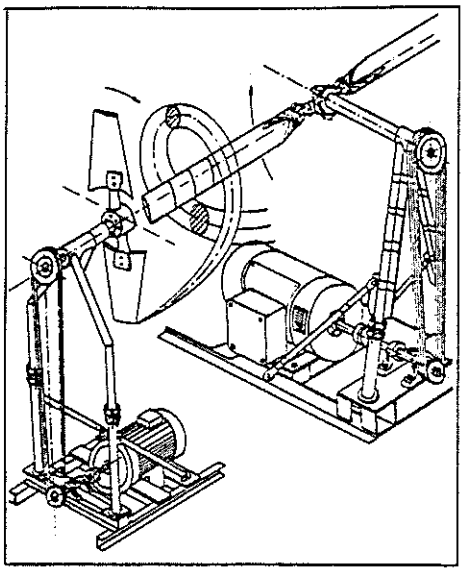

Fig. 2 Test facility

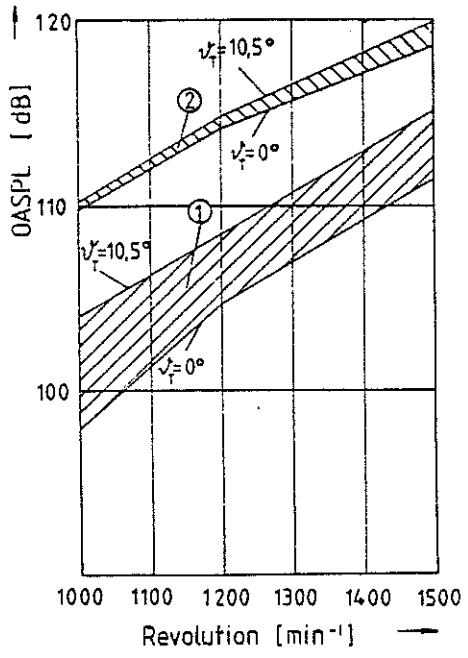

Fig. 3 Overall sound pressure level
Region ① undisturbed tail rotor
Region ② disturbed tail rotor
(n_V=1000rpm, ϑ_V=38°)

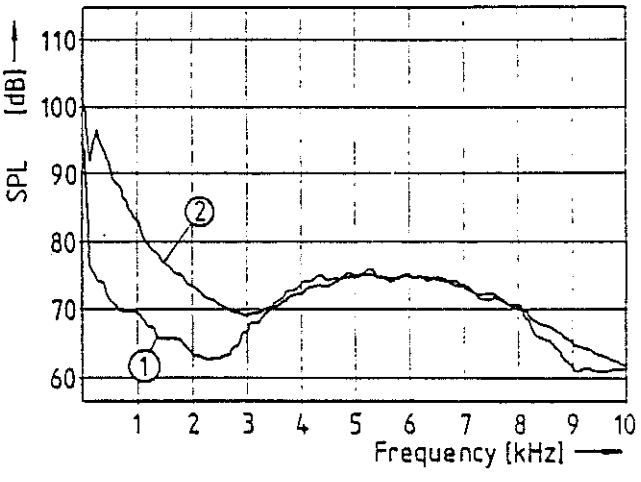

Fig. 4 Frequency spectrum
Graph ① : undisturbed tail rotor
(n_T=1000rpm, ϑ_T=0°)
Graph ② : disturbed tail rotor
(n_T=1000rpm, ϑ_T=0°
n_V=850rpm, ϑ_V=35°)

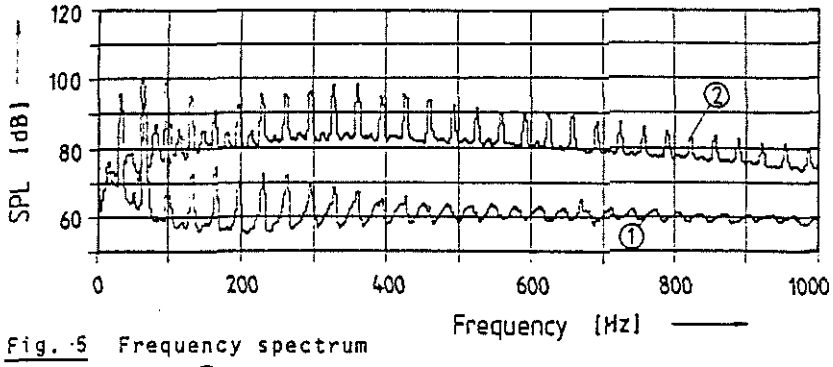

Fig. 5 Frequency spectrum
Graph ① undisturbed tail rotor (n_T=1000rpm, ϑ_T=0°,
Graph ② disturbed tail rotor (n_T=1000rpm, ϑ_T=0°)
(n_V=1000rpm, ϑ_V=38°)

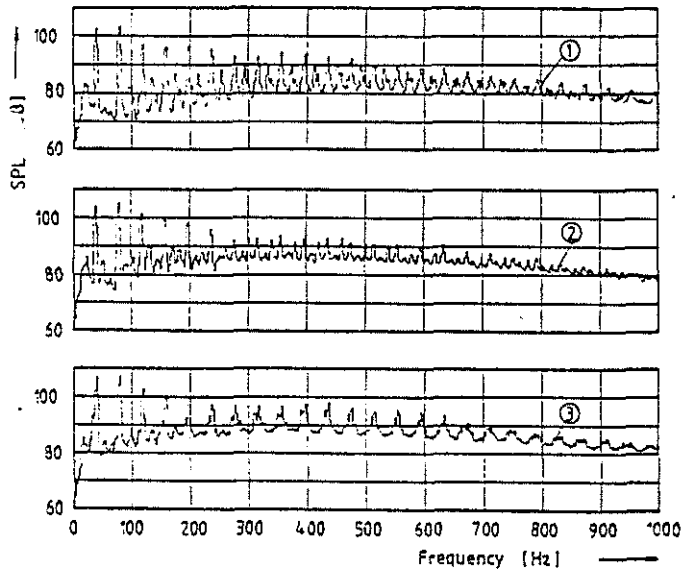

Fig. 6 Frequency spectrum
Graph ① : n_V=500rpm
Graph ② : n_V=750rpm
Gpaph ③ : n_V=1000rpm
(n_T=1200rpm, ϑ_T=10.5°, ϑ_V=38°)

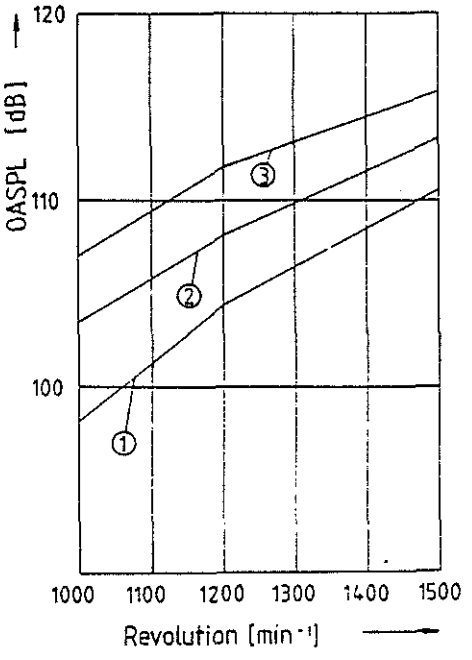

Fig. 7 Overall sound pressure level
Graph ① : undisturbed tail rotor
(ϑ_T=0°)
Graph ② : disturbed tail rotor
(ϑ_T=0°, n_V=750rpm, ϑ_V=25°)
Graph ③ : disturbed tail rotor
(ϑ_T=0°, n_V=750rpm, ϑ_V=38°)

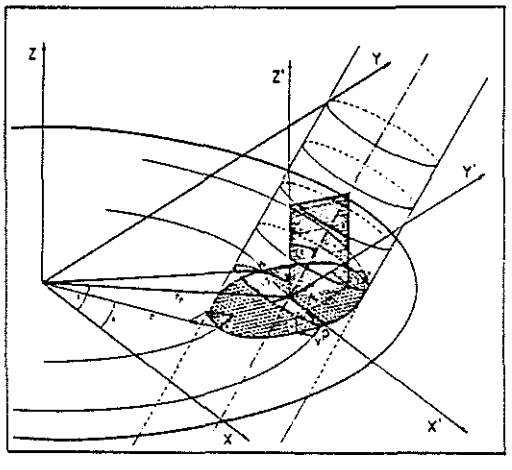

Fig. 8 Vortex in an arbitrary position to the tail rotor plane

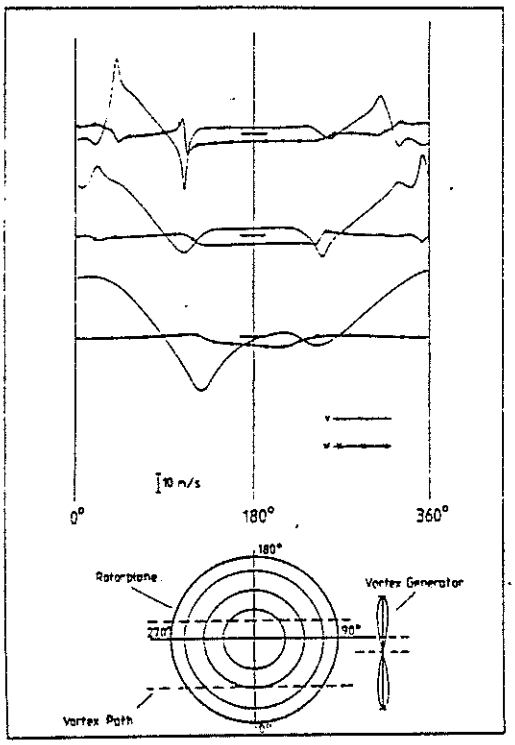

Fig. 9 Components v and w of the velocity distortion for three blade elements

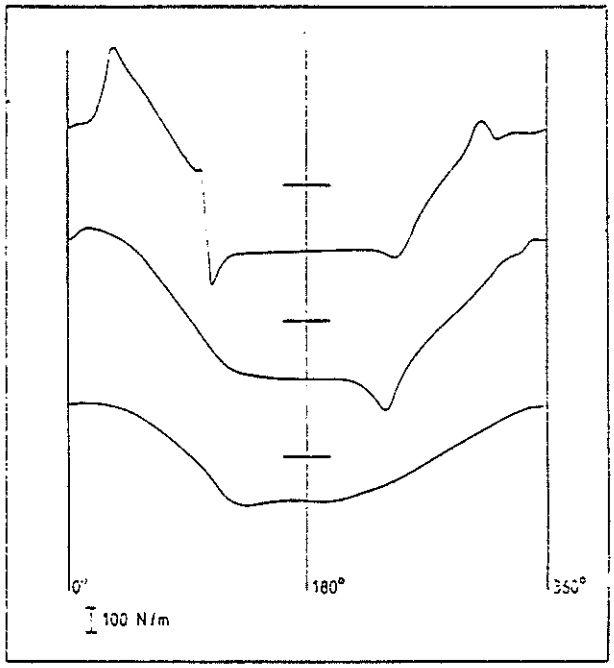

Fig. 10 Unsteady blade forces resulting from the velocity distortion of Fig. 9

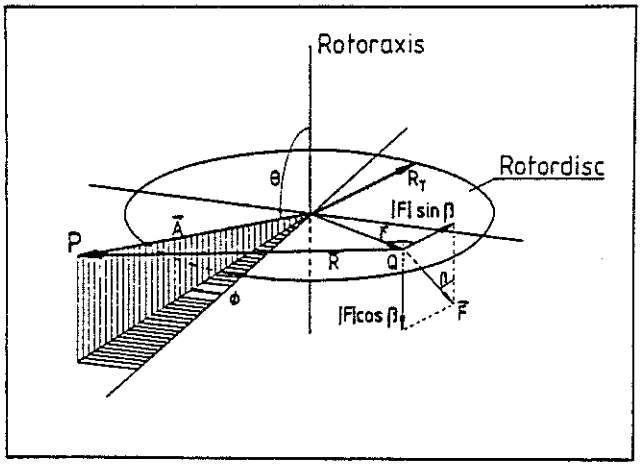

Fig. 11 Coordinate system and nomenclature for the calculation of the sound field

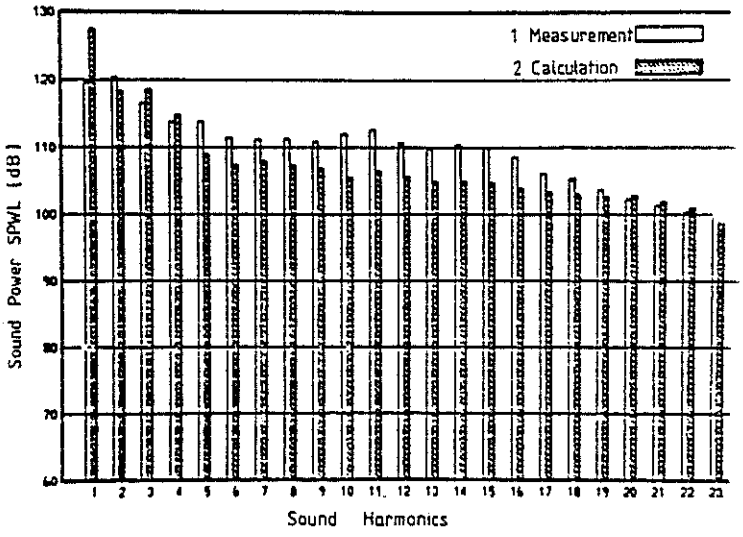

Fig. 12 Comparison of measured and calculated sou pressure levels for the disturbed tail ro (n_T=1200 rpm, ϑ_T=10.5°, n_V=1200rpm, ϑ_V=38°